

Data Mining with Molecular Design Rules Identifies New Class of Dyes for Dye-Sensitised Solar Cells

Jacqueline M. Cole^{a,b*}, Kian Sing Low^a, Hiroaki Ozoe^c, Panagiota Stathi^d, Chitoshi Kitamura^c, Hiroyuki Kurata^e, Petra Rudolf^d, Takeshi Kawase^c

^a Cavendish Laboratory, University of Cambridge, J. J. Thomson Avenue, Cambridge, CB3 0HE. UK.

^b Argonne National Laboratory, 9700 S Cass Avenue, Argonne, IL 60439. USA.

^c Graduate School of Engineering, University of Hyogo, 2167 Shosha, Himeji, Hyogo 671-2280, Japan

^d Zernike Institute for Advanced Materials, University of Groningen, Nijenborgh 4, 9747AG Groningen, The Netherlands

^e Department of Chemistry, Graduate School of Science, Osaka University, Machikaneyama-Cho 1-1, Toyonaka, Osaka, 560-0043, Japan

Author for Correspondence (J. M. Cole): jmc61@cam.ac.uk

Table of Contents

(A) Preparation and Chemical Characterization of **1** and **2**.

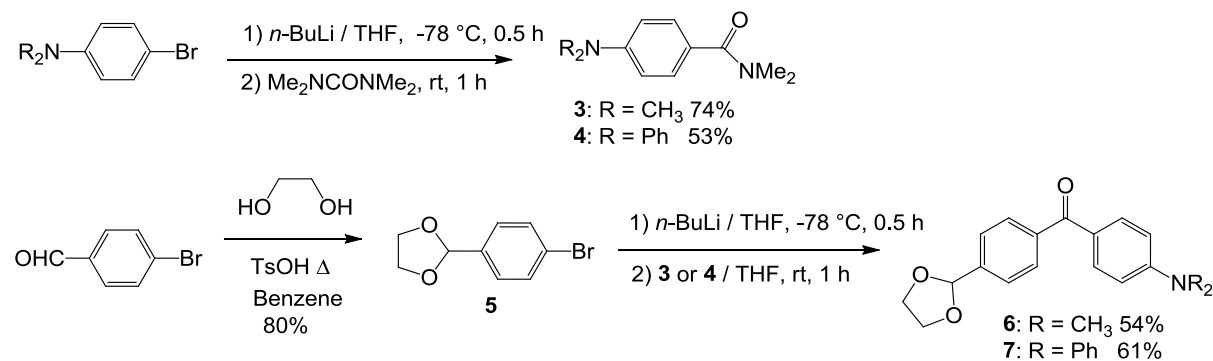
(B) Density Functional Theory and Time-Dependent Density Functional Theory of **1** and **2**

(D) X-ray Photoelectron Spectroscopy of **1** and **2**

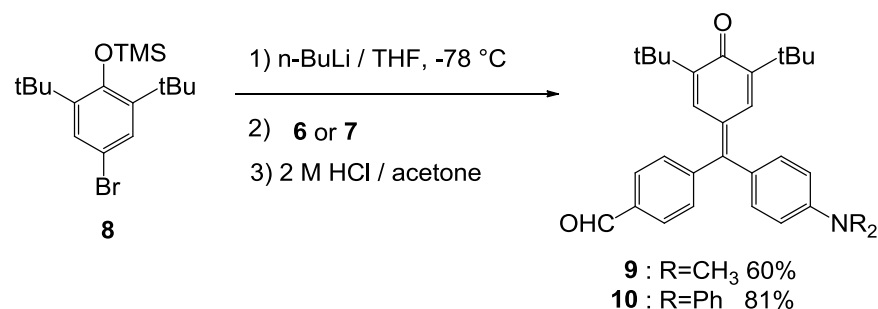
(A) Preparation and Chemical Characterization of 1 and 2

Synthesis Overview

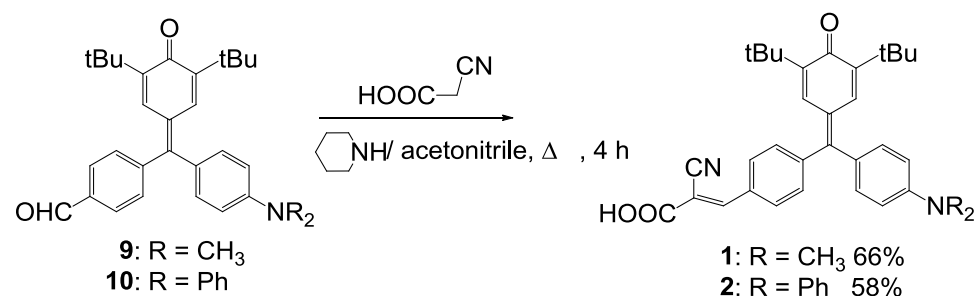
1 and **2** were synthesized by reacting 4-bromo-2,6-di(*t*-butyl)-1-(trimethylsiloxy)benzene **8** with 4-*N,N*-dialkylamino-4'-formylbenzophenone ethylene acetal (where alkyl = methyl **6**^[1] or phenyl **7**^[2]) in the presence of *n*-butyllithium in tetrahydrofuran at -78°C , followed by a Knoevenagel condensation reaction with cyanoacetic acid in acetonitrile³. The key reaction steps are given below:



Scheme 1: Preparation of the benzophenone **6** and **7**.



Scheme 2. Synthesis of quinone methide **9** and **10**.



Scheme 3. Knoevenagel condensation of **9** and **10** to give **1** and **2**.

Experimental Section

General. All the reactions dealing with air- or moisture-sensitive compounds were carried out in a dry reaction vessel under a positive pressure of nitrogen. Air- and moisture-sensitive liquids and solutions were transferred *via* a syringe. Analytical thin-layer chromatography was performed using glass plates pre-coated with Merck Art. 7730 Kiesel-gel 60 GF-254. Thin layer chromatography plates were visualized by exposure to ultraviolet light (UV). Organic solutions were concentrated by rotary evaporation at *ca.* 15 Torr using a diaphragm pump. Column chromatography was performed with Merck Kiesel-gel 60. All reagents were

purchased from Tokyo Kasei Co., Nakarai Tesc., Wako Co. and other commercial suppliers and were used as supplied unless otherwise stated. *n*-Buthyllithium (*n*-BuLi) solution (1.6 M in hexane) was purchased from Mitsuwa Pure Chemicals, Inc.. Anhydrous diethyl ether, toluene and dimethylsulfoxide (DMSO) were purchased from Kanto Chemical Co. and dried where necessary using standard procedures. Tetrahydrofuran (THF) was purchased from Wako Chemical Co. and distilled from lithium aluminum hydride at 760 Torr under a nitrogen atmosphere before used.

Melting points were recorded on a Yanaco MP-S3 apparatus and uncorrected. EI mass spectra were measured on a Shimadzu GCMS-QP5050A. High-resolution mass spectra were measured on a Thermo Fisher Scientific, linear trap quadrupole/orbitrap mass spectrometer (LTQ-Orbitrap XL). ¹H NMR spectra (tetramethylsilane; 0 ppm as an internal standard) and ¹³C NMR spectra (CDCl₃; 77.0 ppm as an internal standard) were recorded on BRUKER DRX-500, and JEOL EX-270 apparatus. The chemical shifts are given in ppm. IR spectra were obtained from Shimadzu FTIR-8400 spectrometer. Electronic (UV-Vis) spectra were obtained on HITACHI U3500 spectrophotometer. Elemental analyses were obtained from Yanaco MT5 CHN corder MT-5. Fluorescence spectra in solution were recorded with a HITACHI F2500 spectrophotometer.

Materials.

4-Bromo-2,6-di(*t*-butyl)-1-(trimethylsiloxy)benzene **8**^[4], 4-bromobenzaldehyde ethylene acetal **5**^[5], 4-*N,N*-dimethylamino-benzamide **3**^[1], 4-*N,N*-diphenylamino-benzamide **4**^[2], and were prepared by reported procedures.

4-*N,N*-dimethylamino-4'-formylbenzophenone ethylene acetal (6)

A solution of **5** (461 mg, 2 mmol) in THF (10 mL) was stirred at -78 °C under N₂. To the solution was added *n*-BuLi (1.3 mL, 2 mmol) via syringe. The reaction mixture was stirred at the temperature for 30 min. Then, to the reaction mixture was added a solution of **3** (386 mg, 2 mmol) in THF (1.5 mL) via syringe. The mixture was allowed to warm at r.t., stirred for an additional 30 min, quenched with sat. NH₄Cl aq, and extracted with toluene. The organic layer was separated, washed with brine, and dried over unhydrous Na₂SO₄. The solvent of the filtrate was evaporated under reduced pressure. The residue was charged with silica gel column chromatography (20 g) to give **6** (324 mg) from toluene/ethyl acetate (9:1) as pale yellow solid in 54% yield. Mp 147.3—148.2 °C; ¹H NMR (270MHz, CDCl₃) δ 7.79 (d, 2H), 7.73 (d, 2H), 7.57 (d, 2H), 6.67 (d, 2H), 5.89 (s, 1H), 4.07—4.17 (m, 4H), 3.08 (s, 6H); ¹³C NMR (125 MHz, CDCl₃) δ 40.04, 65.37, 103.23, 110.50, 124.60, 126.10, 129.49, 132.73, 140.02, 140.70, 153.30, 194.74; IR (KBr) ν/cm⁻¹ 770 (m), 826 (m), 843 (w), 959 (m), 1072 (s), 1150 (m), 1198 (m), 1287 (m), 1323 (m), 1371 (m), 1603 (s), 1638 (s), 2882 (m), 3048 (w); MS (EI) *m/z* 297 (M⁺); Calcd for C₁₈H₁₉NO₃ : C; 72.71, H; 6.44, N; 4.71, : Found: C; 72.47, H; 6.32, N; 4.64.

4-*N,N*-diphenylamino-4'-formylbenzophenone ethylene acetal (7)

A solution of **5** (1.623 g, 7.0 mmol) in THF (12 mL) was stirred at -78 °C under N₂. To the solution was added *n*-BuLi (5.4 mL, 8.4 mmol) via syringe. The reaction mixture was stirred at the temperature for 30

min. Then, to the reaction mixture was added a solution of **4** (2.329 g, 7.0 mmol) in THF (8 mL) via syringe. The mixture was allowed to warm at r.t., stirred for an additional 30 min, quenched with sat. NH₄Cl aq, and extracted with toluene. The organic layer was separated, washed with brine, and dried over anhydrous Na₂SO₄. The solvent of the filtrate was evaporated under reduced pressure. The residue was charged with silica gel column chromatography (25 g) to give **7** (1.784 g) from toluene/ethyl acetate (9:1) as pale yellow solid in 61% yield. Mp 126.5—127.3 °C; ¹H NMR (270 MHz, CDCl₃) δ 7.78 (AA'BB', *J*_{AB} = 7.9 Hz, 2H), 7.68 (AA'BB', *J*_{AB} = 8.7 Hz, 2H), 7.57 (AA'BB', *J*_{AB} = 7.9 Hz, 2H), 7.11—7.36 (m, 10H), 7.00 (AA'BB', *J*_{AB} = 8.7 Hz, 2H), 5.89 (s, 1H), 4.07—4.15 (m, 4H); ¹³C NMR (67.8 MHz, CDCl₃) δ 65.31, 103.07, 119.44, 124.62, 125.93, 126.15, 129.39, 129.56, 129.61, 131.88, 139.11, 141.40, 146.41, 151.94, 194.62; IR (KBr) ν/cm⁻¹ 700 (m), 762 (s), 854 (m), 930 (m), 1084 (s), 1144 (m), 1173 (m), 1279 (s), 1420 (m), 1489 (s), 1582 (m), 1641 (m), 2872 (w), 3036 (w); MS(EI) *m/z* 421 (M⁺); Calcd for C₂₈H₂₃NO₃ : C; 79.79, H; 5.50, N; 3.32, : Found: C; 79.81, H; 5.70, N; 3.20.

7-(4-*N,N*-dimethylaminophenyl)-7-(4-formylphenyl)-2,6-di(*t*-butyl)quinone methide **9**

A solution of **8** (358 mg, 1 mmol) in THF (10 mL) was stirred at -78 °C under N₂. To the solution was added *n*-BuLi (0.7 mL, 1.1 mmol) via syringe. The reaction mixture was stirred at the temperature for 30 min. Then, to the reaction mixture was added a solution of **6** (298 mg, 1 mmol) in THF (8 mL) via syringe. The mixture was allowed to warm at r.t., stirred for an additional 30 min, quenched with sat. NH₄Cl aq, and extracted with toluene. The organic layer was separated, washed with brine, and dried over anhydrous Na₂SO₄. The solvent of the filtrate was evaporated under reduced pressure. The residue was solved with acetone (20 mL) and 2 M hydrochloric acid (2 mL). The mixture was stirred overnight. The resulting dark reddish solution was extracted with toluene, washed with water and brine, and dried over anhydrous Na₂SO₄. The solvent of the filtrate was evaporated under reduced pressure. The residue was charged on silica gel column chromatography (30 g) to give **9** (267 mg) from toluene/ethyl acetate (9:1) as red solid in 60% yield. Mp 237.8—238.9 °C; ¹H NMR (270 MHz, CDCl₃) δ 10.10 (s, 1H), 7.92 (AA'BB', *J*_{AB} = 8.2 Hz, 2H), 7.44 (AA'BB', *J*_{BA} = 8.2 Hz, 2H), 7.37 (s, 1H), 7.10 (AA'BB', *J*_{AB} = 8.9 Hz, 2H), 6.97 (s, 1H), 6.69 (AA'BB', *J*_{BA} = 8.9 Hz, 2H), 3.07 (s, 6H), 1.30 (s, 9H), 1.23 (s, 9H); ¹³C NMR (67.8 MHz, CDCl₃) δ 29.49, 29.65, 35.24, 35.34, 40.07, 111.10, 127.34, 128.90, 129.01, 131.71, 132.26, 132.80, 134.19, 136.22, 146.87, 147.21, 147.88, 151.20, 155.18, 185.93, 191.71; IR (KBr) ν/cm⁻¹ 818(m), 974(m), 1167(m), 1202(m), 1339(m), 1360(s), 1487(s), 1586(s), 1697(m), 2862(w), 2907(w), 2953(m); MS (EI) *m/z* 441 (M⁺); Calcd for C₃₀H₃₅NO₂ : C; 81.59, H; 7.99, N; 3.17, : Found: C; 81.62, H; 7.84, N; 3.15.

7-(4-*N,N*-diphenylaminophenyl)-7-(4-formylphenyl)-2,6-di(*t*-butyl)quinone methide **10**

A solution of **8** (536 mg, 1.5 mmol) in THF (12 mL) was stirred at -78 °C under N₂. To the solution was added *n*-BuLi (1.1 mL, 1.7 mmol) via syringe. The reaction mixture was stirred at the temperature for 30 min. Then, to the reaction mixture was added a solution of **7** (633 mg, 1.5 mmol) in THF (5 mL) via syringe. The mixture was allowed to warm at r.t., stirred for an additional 30 min, quenched with sat. NH₄Cl aq, and extracted with toluene. The organic layer was separated, washed with brine, and dried over anhydrous

Na₂SO₄. The solvent of the filtrate was evaporated under reduced pressure. The residue was solved with acetone (20 mL) and 2 M hydrochloric acid (2 mL). The mixture was stirred overnight. The resulting dark reddish solution was extracted with toluene. The organic layer was washed with water and brine, and dried over anhydrous Na₂SO₄. The solvent of the filtrate was evaporated under reduced pressure. The residue was charged on silica gel column chromatography (30 g) to give **10** (684 mg) from toluene/ethyl acetate (9:1) as red solid in 81% yield. Mp 199.3—200.3 °C; ¹H NMR (270MHz, CDCl₃) δ 10.09 (s, 1H), 7.93 (AA'BB', J_{AB} = 8.2 Hz, 2H), 7.47 (AA'BB', J_{AB} = 8.2 Hz, 2H), 6.99—7.35 (m, 16H), 1.23 (s, 18H); ¹³C NMR (67.8 MHz, CDCl₃) δ 29.43, 29.49, 35.25, 35.33, 120.25, 124.35, 125.57, 129.10, 129.51, 129.95, 131.32, 131.71, 132.35, 132.53, 133.25, 136.18, 146.68, 147.17, 147.48, 147.62, 149.26, 153.75, 185.93, 191.53; IR (KBr) v/cm⁻¹ 698 (m), 756 (m), 822 (m), 1167 (m), 1192 (m), 1207 (m), 1294 (m), 1337 (m), 1362 (m), 1489 (s), 1586 (s), 1705 (s), 2864 (m), 2917 (m), 2955 (m); MS(EI) m/z 565 (M⁺); Calcd for C₄₀H₃₉NO₂ : C; 84.92, H; 6.95, N; 2.48, : Found: C; 85.11, H; 7.22, N; 2.39.

Quinomethide 1

A solution of **9** (177 mg, 0.40 mmol), cyanoacetic acid (39 mg, 0.45 mmol), and piperidine (0.08 mL, 0.8 mmol) with acetonitrile (12 mL) was heated at reflux for 4 h under N₂. A piperidine complex of **1** precipitated as dark red solid. The solid was solved in diethyl ether, and washed with 0.5 M hydrochloric acid and water, and dried over anhydrous Na₂SO₄. The solvent of the filtrate was evaporated under reduced pressure to give crude **1**. It was purified by recrystallization from chloroform/hexane to give pure **1** (134.3 mg) as dark red prisms in 66% yield. Mp 181.2—182.6 °C; ¹H NMR (270MHz, CDCl₃) δ 8.25 (s, 1H), 8.00 (AA'BB', J_{AB} = 8.2 Hz, 2H), 7.35 (AA'BB', J_{BA} = 8.2 Hz, 2H), 7.35 (s, 1H), 7.09 (AA'BB', J_{AB} = 8.9 Hz, 2H), 7.04 (s, 1H), 6.69 (AA'BB', J_{BA} = 8.9 Hz, 2H), 3.07 (s, 6H), 1.30 (s, 9H), 1.23 (s, 9H); ¹³C NMR (125 MHz, CDCl₃) δ 15.12, 29.59, 35.34, 40.27, 102.80, 111.39, 115.20, 127.43, 129.15, 130.77, 131.57, 132.21, 133.24, 134.39, 147.07, 147.23, 151.24, 155.33, 155.47, 166.62, 185.90; IR (KBr) v/cm⁻¹ 814 (w), 968 (w), 1206 (m), 1283 (m), 1339 (m), 1362 (s), 1424 (m), 1489 (m), 1508 (m), 1597 (s), 1705 (m), 2230 (w), 2864 (w), 2915 (w), 2951 (m); MS(ESI) m/z (%) 508 ([M]⁺, 100), 509 (35.7), 510 (6.2); Calcd for C₃₃H₃₆N₂O₃: C; 77.92, H; 7.13, N; 5.51, : Found: C; 77.91, H; 7.28, N; 5.29.

Quinomethide 2

A solution of **10** (175 mg, 0.31 mmol), cyanoacetic acid (29.3 mg, 0.33 mmol), and piperidine (0.06 mL, 0.6 mmol) with acetonitrile (20 mL) was heated at reflux for 4 h under N₂. A piperidine complex of **2** precipitated as dark red solid. The solid was solved in diethyl ether, and washed with 0.5 M hydrochloric acid and water, and dried over anhydrous Na₂SO₄. The solvent of the filtrate was evaporated under reduced pressure to give crude **2**. It was purified by recrystallization from chloroform/hexane to give pure **2** (112 mg) as dark red prisms in 57% yield. Mp 207.3—208.2 °C; ¹H NMR (500 MHz, CDCl₃) δ 8.18 (s, 1H), 7.99 (AA'BB', J_{AB} = 8.2 Hz, 2H), 7.38 (AA'BB', J_{AB} = 8.2 Hz, 2H), 7.32 (m, *meta*-Ph, 4H), 7.30 (d, J = 1.5 Hz, 1H), 7.18 (br. d, *ortho*-Ph, J_{ortho-meta} = 7.8 Hz, 4H), 7.12 (br. t, *para*-Ph, J_{meta-para} = 7.6 Hz, 2H), 7.08 (d, J = 1.5 Hz, 1H), 7.05 (AA'BB', J_{AB} = 8.9 Hz, 2H), 7.02 (AA'BB', J_{BA} = 8.9 Hz, 2H), 1.29 (s, 9H), 1.23 (s, 9H);

^{13}C NMR (67.8 MHz, CDCl_3) δ 29.52, 35.35, 35.40, 114.94, 120.32, 124.34, 125.66, 129.58, 130.32, 130.90, 131.46, 131.86, 132.23, 132.97, 133.37, 146.73, 146.79, 147.80, 149.44, 153.52, 155.60, 186.02; IR (KBr) ν/cm^{-1} 698 (m), 1192 (m), 1285 (m), 1316 (m), 1338 (m), 1362 (m), 1491 (s), 1589 (s), 1717 (m), 2228 (w), 2864 (w), 2926 (w), 2957 (m); MS(EI) $m/z(\%)$ 632($[\text{M}]^+$, 100), 633(46.5), 634(10.6), 635(1.6); HRMS (ESI) Calcd for $\text{C}_{43}\text{H}_{41}\text{N}_2\text{O}_3$: 633.3112; Found m/z = 633.3120.

Crystallographic analysis of **1**.

Single crystals of **1** for X-ray crystallographic analysis were obtained from a *n*-hexane- CHCl_3 solution. The X-ray crystal structure analyses were performed on a Rigaku RAXIS-RAPID Image Plate diffractometer (Mo- $\text{K}\alpha$ radiation, $\lambda = 0.71073 \text{ \AA}$). The structures were solved by direct methods using SIR2004^[6]. The non-hydrogen atoms were refined anisotropically. All hydrogens were located by calculation.

Crystallographic data for **1**: $\text{C}_{33}\text{H}_{36}\text{N}_2\text{O}_3$; Mw = 508.64, $a = 6.1664(3) \text{ \AA}$, $b = 23.5787(9) \text{ \AA}$, $c = 20.6871(7) \text{ \AA}$, $\beta = 99.9610(10)$, $V = 2962.5(2) \text{ \AA}^3$, monoclinic, Space group $P2_1/c$ (#14), Z value = 4, μ (Mo $\text{K}\alpha$) = 0.73 cm^{-1} , $T = 223 \text{ K}$, $D_{\text{calc}} = 1.140 \text{ g/cm}^3$, $F(000) = 1088$, $R1 = 0.0823$, $wR2$ (all data) = 0.3128, GOF = 1.136, Refl./param. = 6741/345 from a total number of 28,339 reflections.

Cyclic voltammetry

Table S2: Electrochemical properties of **1** and **2**, where $^{\text{ox}}E$ and $^{\text{red}}E$ are the formal oxidative and reductive potentials which sum to $E_{0.0}$

compound	$^{\text{ox}}E$ (V)	$^{\text{red}}E$ (V)	HOMO (eV) (obs.)	LUMO (eV) (obs.)	$E_{0.0}$ (eV) (obs.)
1	+0.41	-1.68	-5.12	-3.03	2.09
2	+0.57	-1.69	-5.28	-3.02	2.26

V vs. Ag/Ag^+ , in 0.1 M $\text{Bu}_4\text{NClO}_4/\text{CH}_2\text{Cl}_2$, scan rate 100 mV/s, +25 °C, $\text{Fc}/\text{Fc}^+ = 0 \text{ V}$.

Cyclic voltammograms were acquired using a three-electrode cell equipped with a glassy carbon working electrode ($\varnothing = 3 \text{ mm}$), a platinum wire as a counter-electrode, and an Ag/AgNO_3 reference on a BAS CV-50W Electrochemical Analyser. Before data acquisition, solutions were systematically degassed by bubbling nitrogen for five minutes. The constancy of the reference electrode potential was also checked by measuring the oxidation potential of a ferrocene solution before and after the different studies.

(B) Density Functional Theory and Time-Dependent Density Functional Theory of **1** and **2**

Density functional theory (DFT) calculations and time-dependent DFT was performed on **1** and **2** using the Gaussian09 program package⁷.

DFT and TDDFT computational details

The structures of **1** and **2** were geometry optimised using the B3LYP exchange-correlation functional⁸ and a 6-31G(d) basis set in accordance with benchmarking tests⁹. The starting molecular structure for **1** was taken from X-ray diffraction data (vide infra). The molecular moiety of **1** that is common to **2** was also used as a building block to generate the starting structure of **2** using a combination of Materials Studio 4.4¹⁰ and Avogadro¹¹. All calculations included solvation effects due to methanol (the solvent used for dye solutions in DSC device fabrication) by means of the Polarizable Continuum Model (PCM)^{12,13} implemented in Gaussian09⁷. This has been shown in the literature to be essential in successfully describing the excited-state properties of a series of organic dyes for solar cell applications⁹.

It is worth noting that in both the DFT geometry optimised and X-ray diffraction derived structures for **1**, the three benzene rings arrange not only in an out-of-plane fashion to minimize steric hindrance, but also have good conformational similarity (Figure S2).

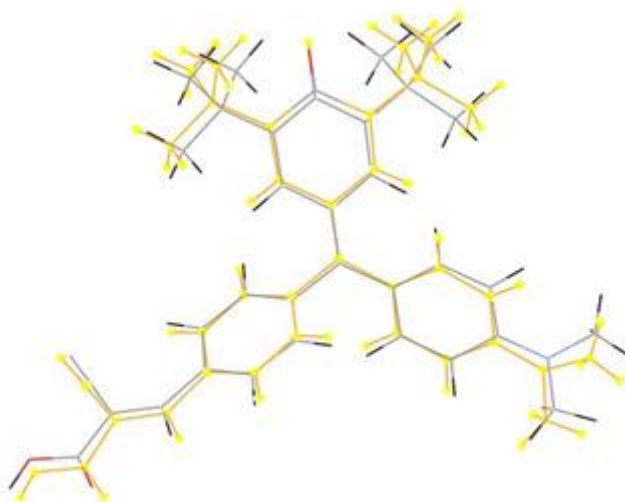


Figure S2: Overlay of X-ray diffraction derived structure of **1** (orange) with that of its DFT geometry optimised structure. Figure was created using Mercury's crystal packing feature tool^{14,15} on all non-hydrogen atoms giving a root mean squared deviation of 0.427 Å.

Furthermore, as can be seen from Table S3, there is a good correlation between bond angles in this area.

Table S3: Comparison of bond angles in **1** experimental and DFT geometry optimised structures

Bond angle	1 (X-ray Diffraction data)	1 (DFT geometry optimised value)
C021 – C028 – C017	122.50°	120.42°
C021 – C028 – C018	124.7°	122.96°

DFT calculations, using the geometry-optimised structure with the B3LYP functional and a 6-31++G(d,p) basis set, were used to investigate the frontier orbitals and calculate the HOMO energy level of both dyes. The M06-2X functional and 6-311+G(d,p) basis set were used for subsequent TDDFT calculations. The M06-2X functional was chosen as it gives good predictions for charge transfer excitations with intermediate spatial overlap and also it performs better than the range-separated CAM-B3LYP functional in these cases¹⁶. The TDDFT calculations included the 6 lowest singlet-singlet transitions up to an energy of 4.26 eV (290 nm). Within this energy range, there were three transitions with appreciable oscillator strength ($f > 0.1$) for both **1** and **2**.

DFT and TDDFT Results

Details of the three optical transitions in **1** and **2** that have appreciable oscillator strength ($f > 0.1$) are given in Tables S4 and S5.

Table S4: TDDFT excitation energies (eV, nm), oscillator strengths (f), composition of molecular orbital contributions and character of **1**, as compared to experimental peak absorption maxima.

n	E (eV, nm)	f	Composition	Character	Experimental
1	2.499(496.11)	0.65	45% HOMO \rightarrow LUMO	CT	499
3	3.345(370.66)	0.85	24% HOMO-1 \rightarrow LUMO	$\pi-\pi^*$	372
4	3.484(355.82)	0.48	23% HOMO \rightarrow LUMO+1	$\pi-\pi^*$	321

Table S5: TDDFT excitation energies (eV, nm), oscillator strengths (f), composition of molecular orbital contributions and character of **2**, as compared to experimental peak absorption maxima.

n	E (eV, nm)	f	Composition	Character	Experimental
1	2.572(482.06)	0.72	43% HOMO \rightarrow LUMO	CT	481
3	3.294(376.44)	0.95	34% HOMO-1 \rightarrow LUMO	$\pi-\pi^*$	371
4	3.495(354.79)	0.39	32% HOMO \rightarrow LUMO+1	$\pi-\pi^*$	300

As can be seen from Tables S4 and S5 and associated spectral renderings with experimental UV/vis absorption spectra overlays (Figures S3 and S4), there is good agreement between experimental and calculated UV/vis peak absorption wavelengths. Also the peak absorption for **1** and **2**, at 499 nm and 481 nm respectively, are assigned to a HOMO-to-LUMO charge-transfer (CT) excitation. The corresponding isodensity plots of the frontier molecular orbitals are shown in Figure S5. TDDFT was used to estimate the associated molecular orbital energy of the LUMO, as it were found to give excellent comparison with experimental Cyclic Voltammetry data (vide infra).

The next two calculated excitations in both **1** and **2** (n=3 and 4) appear to come from two overlapping π - π^* transitions of different character. For **1**, the transition at 3.35 eV is the π - π^* transition from HOMO-1 to the LUMO, reflecting charge-density redistributions between the D- π -A and π -Ads moieties. The less intense peak at 3.48 eV arises from a π - π^* transition from HOMO to LUMO+1 and corresponds to similar optical excitation characteristics. Associated isodensity plots for **1** are given in Figure S6.

Similar charge-redistribution characteristics present for **2** upon optical excitation, except that its π - π^* transition from HOMO to LUMO+1 corresponds to excitation centred more within the tricyclohexylamine group. This analysis is in accordance with the similar structured JK dyes and the assigned composition and character of the molecular orbital transitions¹⁷.

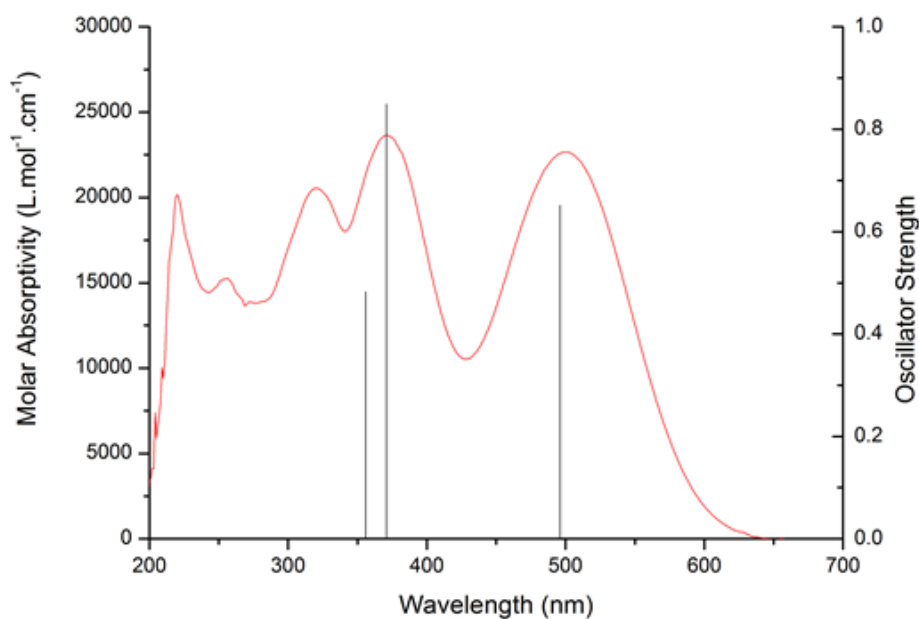


Figure S3: TDDFT generated excitation energies (black lines) with corresponding oscillator strengths of **1** (modeled in methanol solution), in comparison to its experimental UV/vis absorption spectrum (red) in methanol solution.

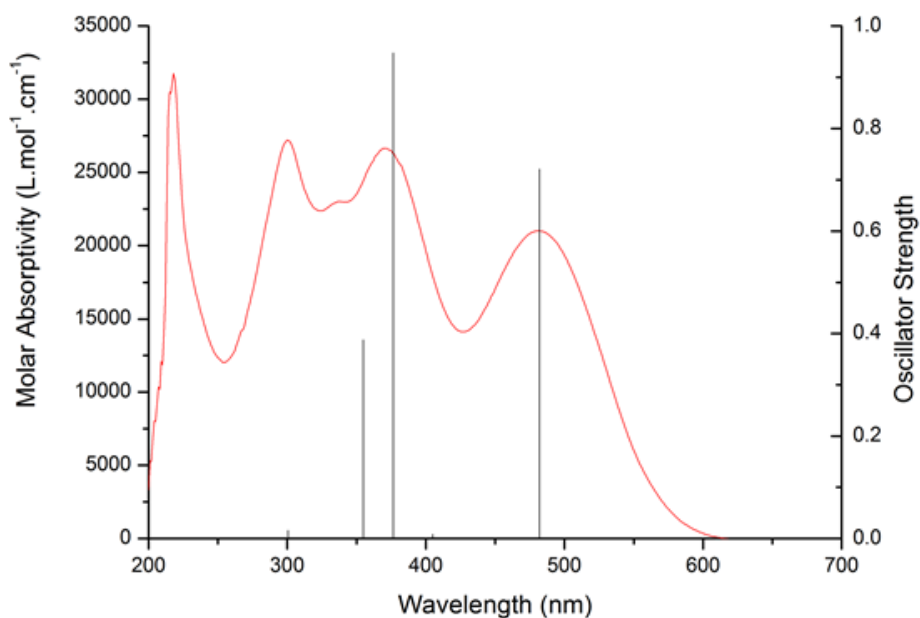


Figure S4: TDDFT generated excitation energies (black lines) with corresponding oscillator strengths of **2** (modeled in methanol solution), in comparison to its experimental UV/vis absorption spectrum (red) in methanol solution.

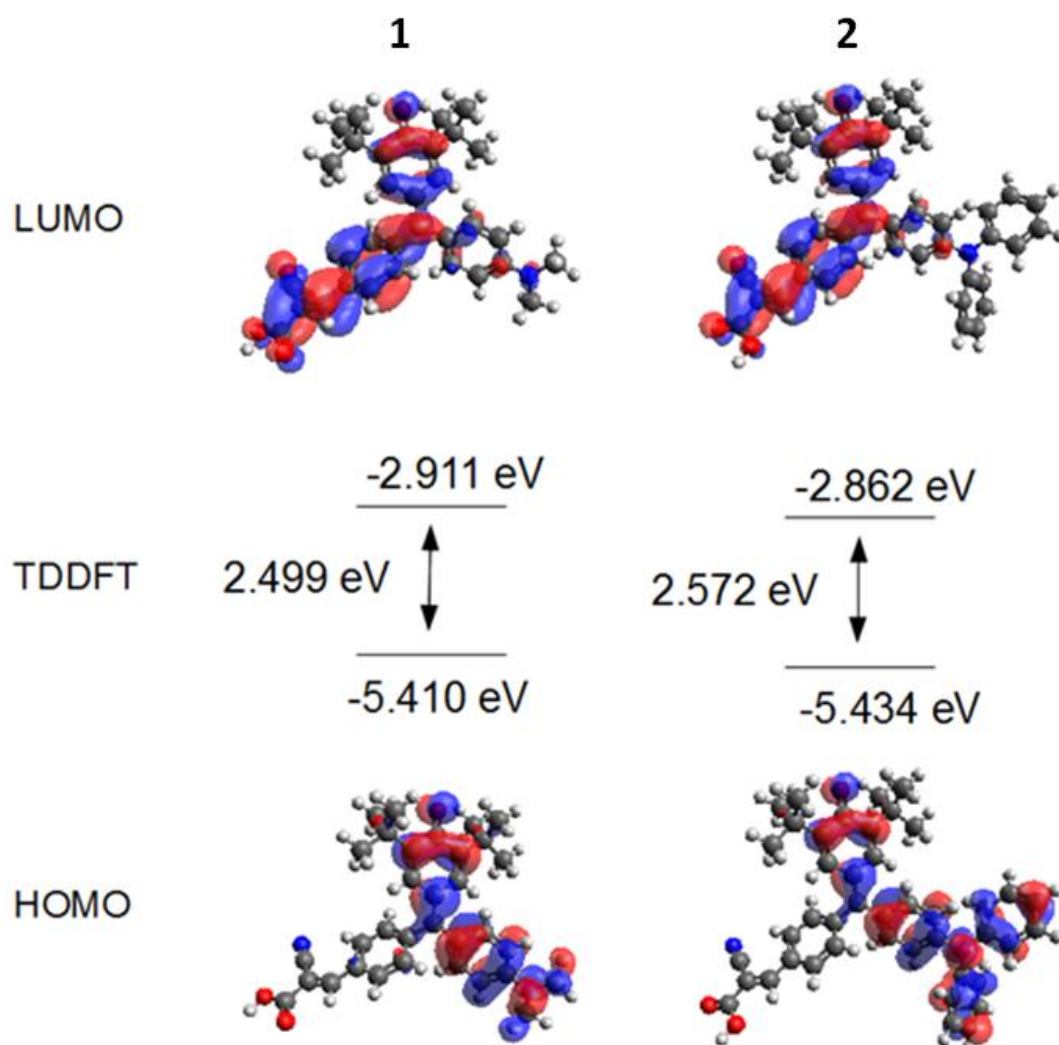


Figure S5: Showing isodensity plots of the HOMO and LUMO levels for **1** and **2**, HOMO and LUMO orbital energies and TDDFT first excitation energies.

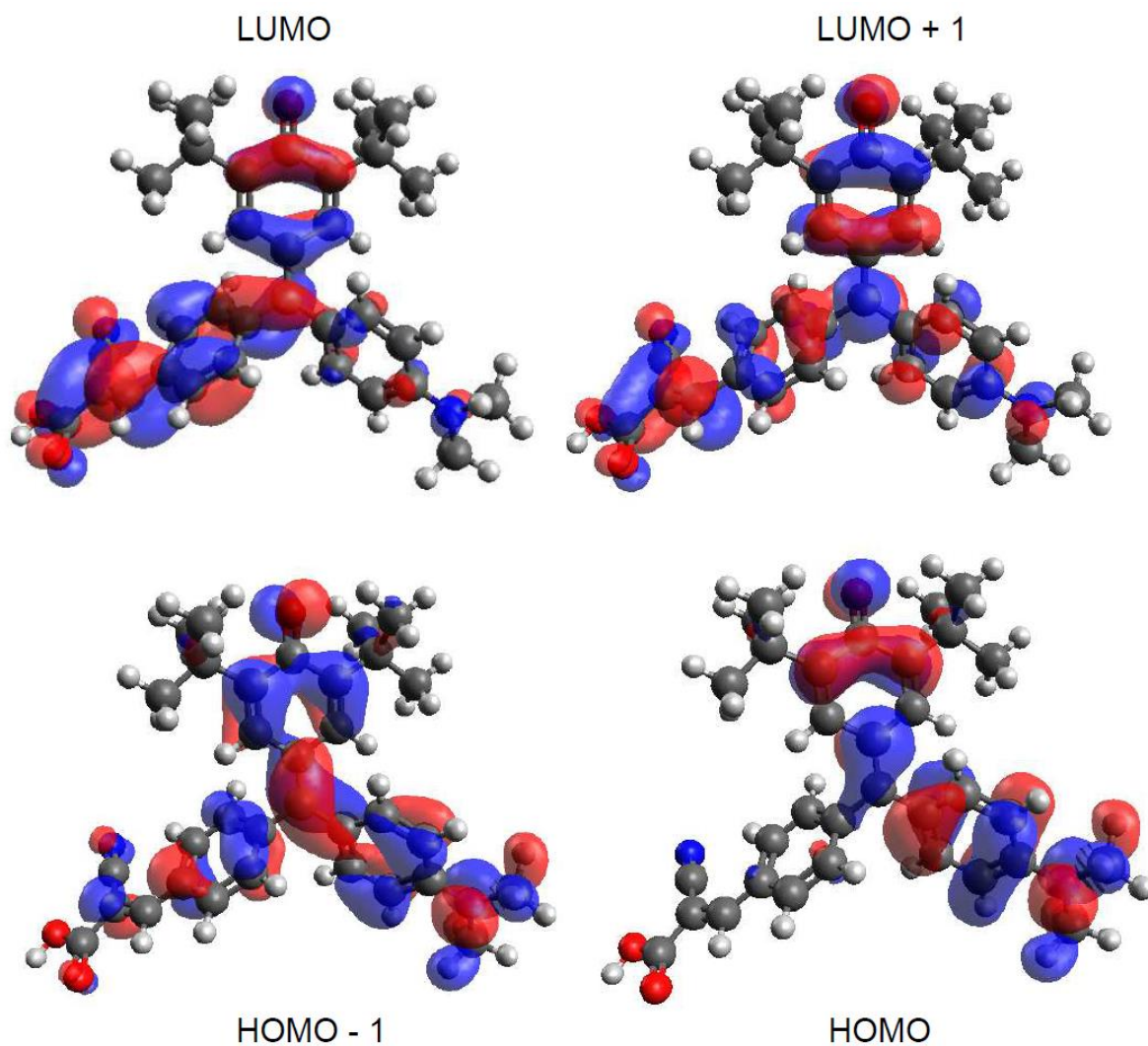


Figure S6: Isodensity plots of HOMO-1 to LUMO and HOMO to LUMO+1 transitions in **1**, with isodensity value 0.02

(C) X-ray Photoelectron Spectroscopy of 1 and 2

XPS Sample Preparation and Experimental Methods

Samples for **1** and **2** were prepared to a 0.7 mM concentration using methanol as a solvent. These dyes were then both drop cast and sensitized onto a $\sim 5\mu\text{m}$ thick film of TiO_2 nanoparticles prepared by the doctor-blade method. The samples were stored in an Atmos glove bag, supplied by Sigma Aldrich, filled with nitrogen gas overnight. The oxygen-free atmosphere was used for sensitization of TiO_2 and non- TiO_2 covered substrates in order to ensure no contamination of the samples; this way, oxygen 1s spectra could easily be related to the interaction of dye with TiO_2 . The sample substrates used were silicon and FTO coated glass for both dye-only spectra and dye-sensitized TiO_2 spectra. Bare TiO_2 substrates were also prepared to act as a reference.

The samples were analysed via XPS at the Zernike Institute for Advanced Materials, University of Groningen, Netherlands. XPS data were collected using a Surface Science Instruments SSX-100 photoelectron spectrometer with a monochromatic $\text{Al K}\alpha$ X-Ray source ($h\nu=1486.6$ eV) operating at a base pressure of $\sim 3\times 10^{-10}$ mbar. The spectra were recorded with an electron take-off angle of 37° with respect to the surface normal on a spot with a diameter of $600\ \mu\text{m}$. The energy resolution was set to 1.26 eV. XPS spectra were analysed using the least-squares curve fitting program Winspec developed at the LISE laboratory, University of Namur, Belgium. Binding energies are reported ± 0.1 eV and referenced to the Carbon 1s photoemission peak, centered at 285.2 eV¹⁸.

Deconvolution of the spectra included background subtraction (Shirley baseline) and fitting with a minimum number of peaks consistent with the structure of the molecules on a surface, taking into account the experimental resolution. The profile of the peaks was taken as a convolution of Gaussian and Lorentzian functions. All measurements were carried out on freshly prepared samples. Three different spots were measured on each surface to check for reproducibility.

XPS Results and Discussion

Titanium 2p

Figure S7 shows the Ti 2p XPS spectrum for an unsensitised TiO_2 film, prepared as above. For the bare TiO_2 films, the effects of spin-orbit coupling splitting of the peaks are observed. The peak at 459.0 eV is attributed to the Ti^{4+} $2p_{3/2}$ state and the peak at 464.8 eV to that of Ti^{4+} $2p_{1/2}$. These two peaks evidence that the oxide surface consists mainly of titanium (IV) dioxide without suboxides present. These peak binding energies correlate well with previously published data and database values (458.7 eV and 464.7 eV)¹⁹⁻²¹.

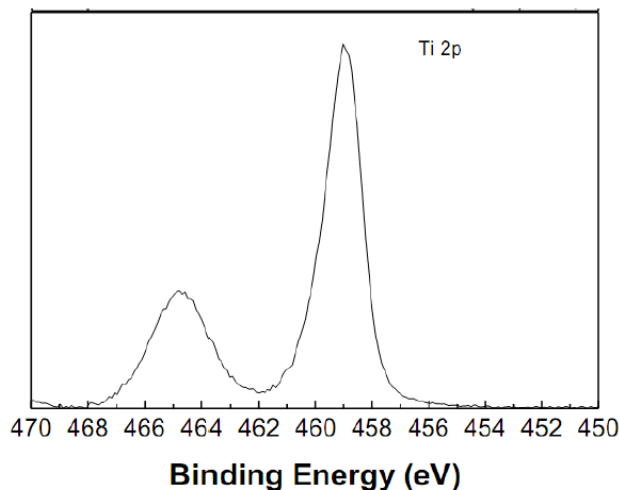
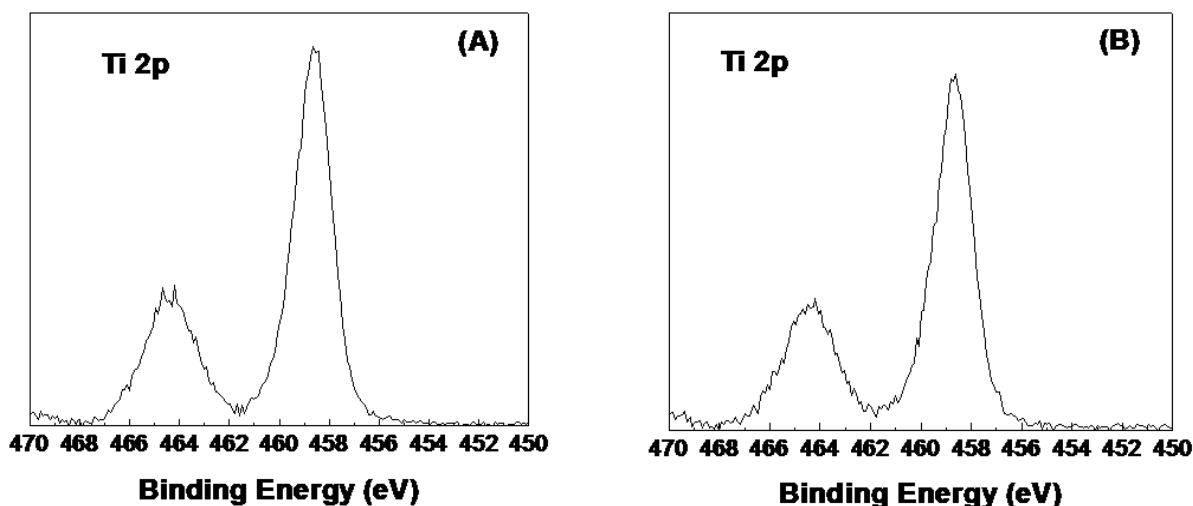


Figure S7: Titanium 2p XPS spectra of TiO₂.

Figure S8 Titanium 2p XPS spectra of (A) 1 on TiO₂ and (B) 2 on TiO₂



The Ti 2p XPS spectra in Figure S8 show a shift to lower binding energies when either **1** or **2** is attached to TiO₂ compared to the case of bare TiO₂. The Ti 2p_{3/2} and Ti 2p_{1/2} peaks are shifted by -0.3 eV and -0.2 eV, respectively, from the non-sensitized TiO₂ peaks. These shifts are attributed to a change in dipole moment of the dye at the surface of TiO₂, owing to the oxygen in the COOH group of the dye losing its hydrogen and forming a Ti-O bond; this leaves the oxygen atom slightly negative due to its higher electronegativity compared with titanium²². As XPS is sensitive to the changes in the surface of the sample, these shifts provide evidence of strong dye attachment to the TiO₂ surface. Indeed, these shifts are common in the literature and have been seen in many interactions of various chromophores with TiO₂^{23,24}.

Oxygen O1s

The O1s XPS spectra allow the investigation of bonding interactions and surface geometrical structure for carboxylated molecules, such as **1** and **2**.

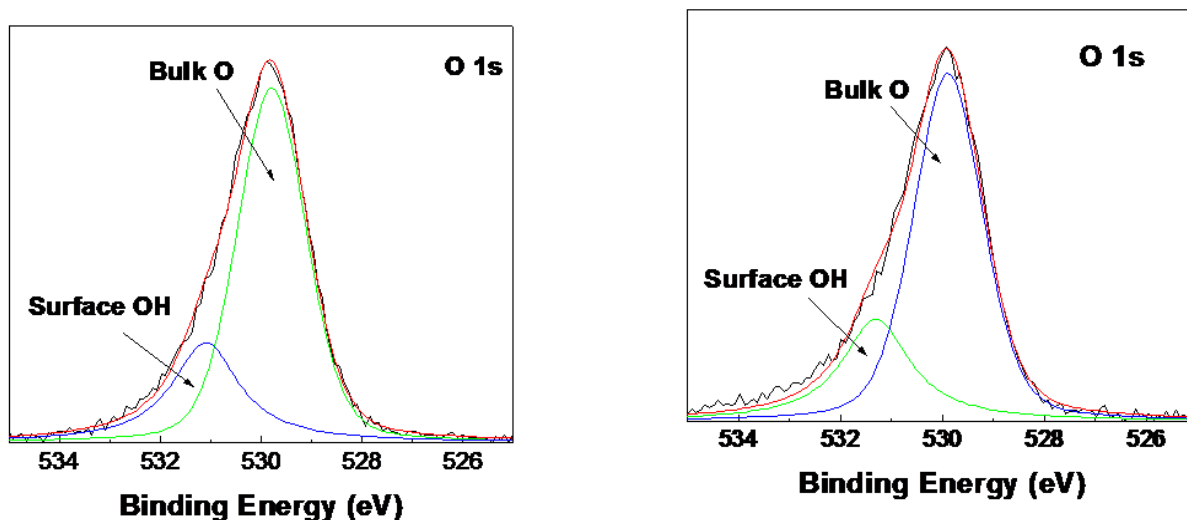


*Figure S9: Oxygen 1s XPS spectra of (A) **1** on TiO₂ and (B) **2** on TiO₂*

For the O1s XPS spectra of dyes **1** and **2** on TiO₂ (Figure S9), there is a shift of 0.2 eV to lower binding energy in comparison to the non-sensitised O1s TiO₂ spectra. The peaks of the sensitised **1** and **2** O1s spectra in Figure S9 were deconvoluted into two components, following the work of Simmons and Beard²⁵. In non-sensitised TiO₂, the bulk oxygen was found at 530.6 eV²⁶ and surface Ti...HO groups were found at 532.5 eV. For both **1** and **2** sensitised TiO₂ layers, the bulk oxygen is observed at 530.4 eV²⁶ and the peak at 532.2 eV is assigned to surface OH groups along with interaction from the -OH in the dyes (532.4 eV²⁷).

Carbon 1s

The C 1s spectrum of **1** sensitised on TiO₂ can be deconvoluted using three components (Figure S10). The C-C bonds are assigned to the peak at 285.0 eV²⁸, C-N or C-O bonds produce the peak at 286.3 eV²⁹⁻³⁰ while the 289.7 eV peak is derived from the COO⁻ group³⁰. The C 1s spectrum for **2** is deconvoluted into two components that relate to C-C bonds at 285 eV²⁸, and the COO⁻ group again at 289.7 eV³⁰.

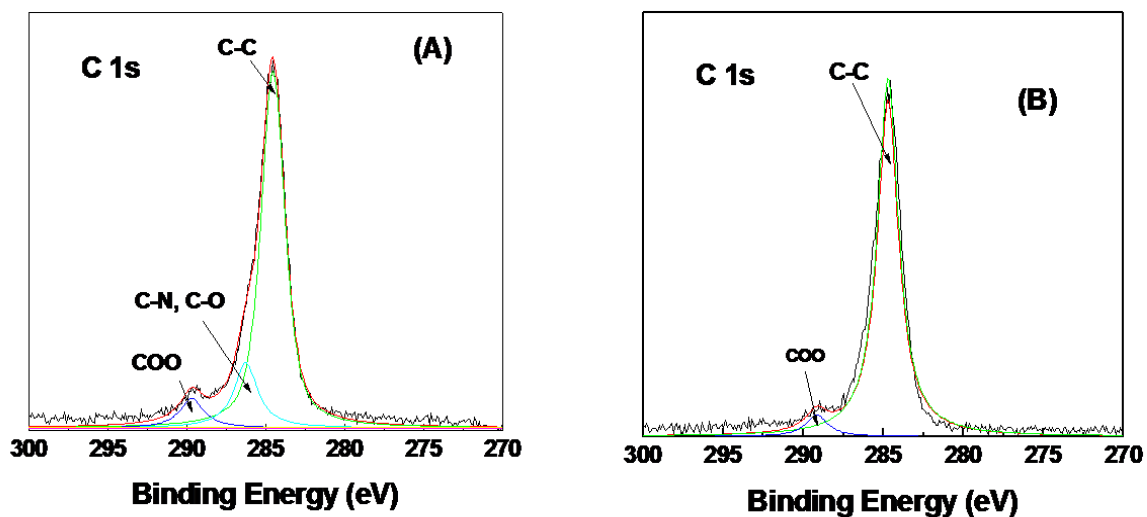


Figure S10: Carbon 1s XPS spectra of (A) **1** on TiO_2 and (B) **2** on TiO_2

Nitrogen 1s

The N 1s line for both dye-sensitized TiO_2 with **1** and **2** peaks at 399.3 eV due to the presence of the CN group²⁹ (Figure S11).

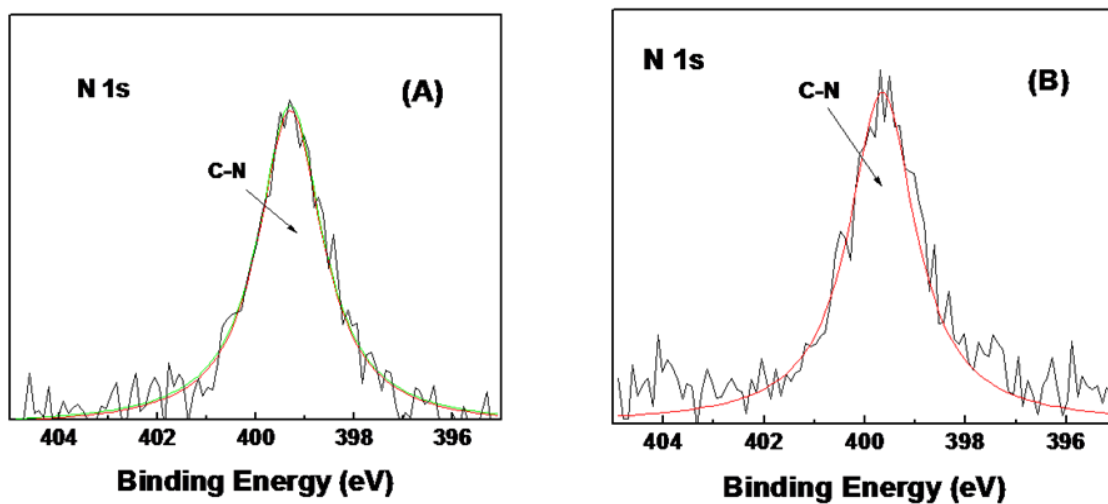


Figure S11: Nitrogen 1s XPS spectra of (A) **1** on TiO_2 and (B) **2** on TiO

References

- [1] T. Kumagai, T. Anki, T. Ebi, A. Konishi, K. Matsumoto, H. Kurata, T. Kubo, K. Katsumoto, C. Kitamura, T. Kawase, *Tetrahedron* **2010**, 66, 8968.
- [2] G. P. Schiemenz, G. Stein, *Tetrahedron*, **1970**, 26, 2007.
- [3] D. P. Hagberg, T. Marinado, K. M. Karlson, K. Nonomura, P. Qin, G. Boschloo, T. Brinck, A. Hagfeldt, L. Sun, *J. Org. Chem.* **2007**, 72, 9550.
- [4] R. Suzuki, H. Kurata, T. Kawase, M. Oda, *Chemistry Lett.*, **1999**, 571.
- [5] Y. Kuramochi, A. S. D. Sandanayaka, A. Satake, Y. Araki, K. Ogawa, O. Ito, Y. Kobuke, *Chem. Eur. J.* **2009**, 15, 2317.
- [6] M. C. Burla, R. Caliandro, M. Camalli, B. Carrozzini, G. L. Casciarano, L. De Caro, C. Giacovazzo, G. Polidori, R. Spagna, *J. Appl. Cryst.* **2005**, 38, 381.
- [7] M. J. Frisch, G. W. Trucks, H. B. Schlegel, G. E. Scuseria, M. A. Robb, J. R. Cheeseman, G. Scalmani, et al. Gaussian09. Gaussian, Inc., Wallingford CT, **2009**.
- [8] A. D. Becke, *J. Chem. Phys.* **1993**, 98, 5648.
- [9] M. Pastore, E. Mosconi, F. De Angelis, M. Graetzel, *J. Phys. Chem. C*, **2010**, 114, 7205.
- [10] Accelrys. Materials Studio 4.4. **2008**.
- [11] Avogadro: an open-source molecular builder and visualization tool. Version 1.0.3.
- [12] S. Miertus, E. Scrocco, J. Tomasi, *Chem. Phys.* **1981**, 55, 117.
- [13] D. M. Chipman, *J. Chem. Phys.* **2000**, 112, 5558.
- [14] Z. F. Weng, W. D. S. Motherwell, J. M. Cole, *J. Appl. Cryst.* **2008**, 41, 955.
- [15] Z. F. Weng, W. D. S. Motherwell, F. H. Allen, J. M. Cole, *Acta Cryst. B* **2008**, 64, 348.
- [16] R. Li, J. Zheng, D. G. Truhlar, *Phys. Chem. Chem. Phys.* **2010**, 12, 12697.
- [17] S. Kim, J. K. Lee, S. O. Kang, J. Ko, J. Yum, S. Fantacci, F. Angelis, D. Di Censo, M. K. Nazeeruddin, M. Graetzel, *J. Am. Chem. Soc.*, **2006**, 128, 16701.

- [18] J. F. Moulder, W. F. Stickle, P. E. Sobol, Handbook of X-Ray Photoelectron Spectroscopy; Perkin-Elmer, Physical Electronics Division, **1993**.
- [19] A. Y. Lee, D. M. Blakeslee, C. J. Powell, J. R. Rumble, *Data Science Journal* , **2002**, 1.
- [20] S. O. Saied, J. L. Sullivan, T. Choudhury, C. G. Pearce, *Vacuum* **1988**, 38, 917.
- [21] W. Slinkard, P. Degroot, *Journal of Catalysis* **1981**, 68(2), 423.
- [22] S. Agrawal, N. J. English, K. R. Thampi, J. M. D. Macelroy, *Phys. Chem. Chem. Phys.* **2012**, 14(35), 12044.
- [23] E. M. J. Johansson, M. Hedlund, H. Siegbahn, H. Rensmo, *J. Phys. Chem. B* **2005**, 109, 22256.
- [24] E. M. J. Johansson, M. Hedlund, M., Odelius, H. Siegbahn, H. Rensmo, *J. Chem. Phys.* **2007**, 126, 244303.
- [25] G. W. Simmons, B. C. Beard, *J. Phys. Chem.* 1987, 91, 1143.
- [26] M. Takagi-Kawai, M. Soma, T. Onishi, K. Tamaru, *Canadian Journal of Chemistry* **1980**, 58, 2132.
- [27] G. Jin, R. Park, H. Park, J. Seo, S. Lee, M. Lee, *Chinese Medical Journal* **2010**, 123, 3132.
- [28] G. Beamson, D. Briggs, High Resolution XPS of Organic Polymers: The Scienta ESCA300 Database. Wiley: New York, **1992**.
- [29] M. Barber, J. A. Connor, M. F. Guest, I. H. Hillier, M. Schwarz, M. Stacey, *J. Chem. Soc., Faraday Trans.* **1973**, 4, 551.
- [30] U. Gelius, P. F. Hedén, J. Hedman, B. J. Lindberg, R. Marine, R. Nordberg, C. Nordling, K. Siegbahn, *Physica Scripta* **1970**, 2, 70.